Supplement of

Exploring the Applicability and Limitations of Selected Optical Scattering Instruments for PM Mass Measurement

Jie Zhang*, Joseph P. Marto, James J. Schwab

Correspondence to：jzhang35@albany.edu

S1 Estimate aerosol density used for SMPS

The density of ambient aerosol was calculated based on organic, SO_4, NO_3, and NH_4 mass concentration measured by AMS (Qi Zhang et al. 2005). It assumes that the organic composition had an averaged density of 1.20 g cm^{-3}, and that SO_4 and NO_3 were both components of salts, $(NH_4)_2SO_4$ (density 1.79g cm^{-3}) and NH_4NO_3 (density 1.72g cm^{-3}) respectively (Lee et al. 2015). The averaged ambient density was then calculated by:

$$\rho_{ambient} = \frac{m_{Total}}{\frac{m_{organic}}{\rho_{organic}} + \frac{m_{SO_4}}{\rho_{(NH_4)_2SO_4}} \times \frac{132}{96} + \frac{m_{NO_3}}{\rho_{NH_4NO_3}} \times \frac{80}{62}}$$

Where $\boldsymbol{\rho}$ is density, and $\boldsymbol{m}$ is the mass concentration.

S2 Figures

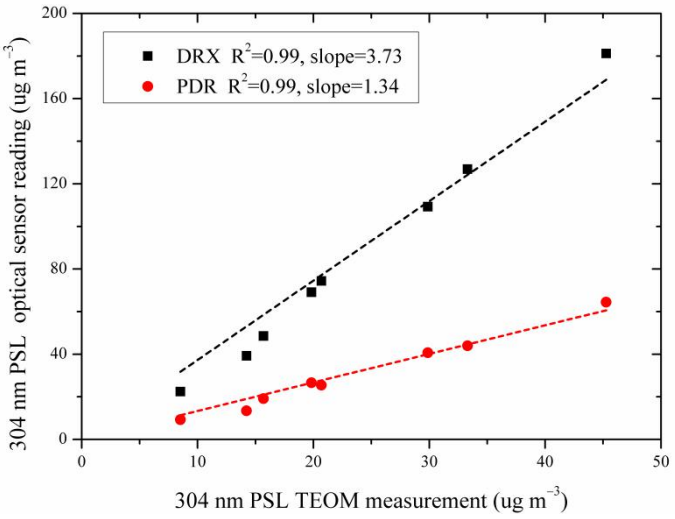

Figure S1. The correlation between the reported mass concentration by optical sensors (DRX and PDR) and by TEOM.

In this study, the reading of OPC-N2 is not included. The OPC-N2 did not produce a response for the 304 nm and smaller PSL particles because of its 380 nm detection limit.

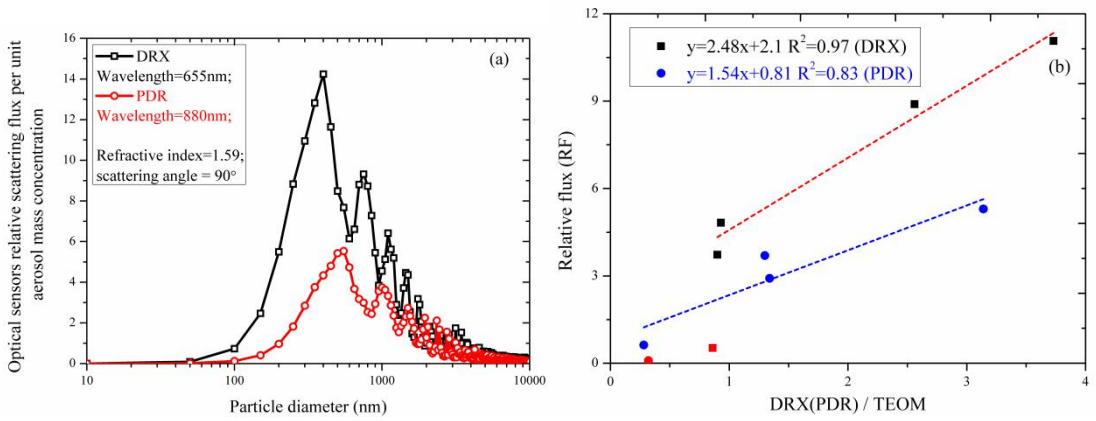

Figure S2. (a): Results of a Mie scattering calculation for conditions appropriate to the DRX (black) and PDR (red); (b) : Correlation between the relative flux with the ratio of optical instruments to TEOM (DRX: black; PDR: blue; and red points relates with the result of 90 nm PSL).

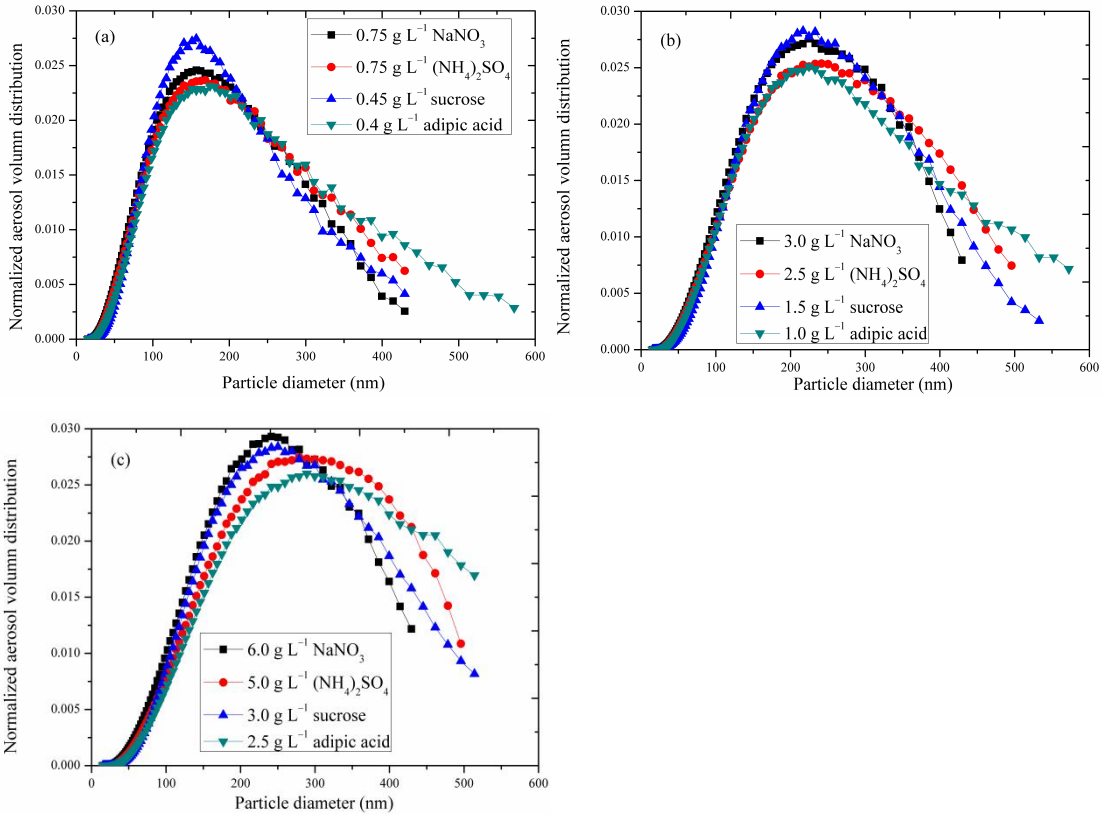

Figure S3. The normalized volume distribution of three aerosol groups. (a): Group 1, with low concentration dilutions; (b): Group 2, with medium concentration dilutions; (c): Group 3, with high concentration dilutions.

In this study, the volume concentration for each bin is divided by total integrated value for all bins to obtain normalized volume concentration, which shows the size distribution of different particles. Figure S3 shows the shift in volume distributions for liquid samples with increasing concentration dilution. As the concentration increases, the volume distribution shifted rightward towards larger particles.

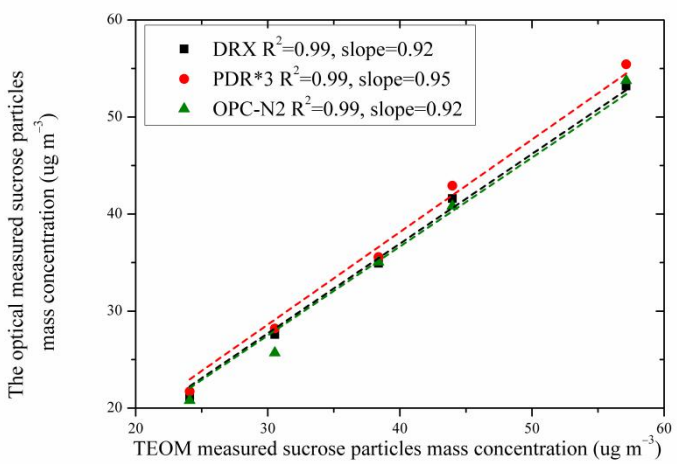

Figure S4. Correlation between the readings of optical sensors and the reference TEOM measurement for 0.45 g L^{-1} sucrose.

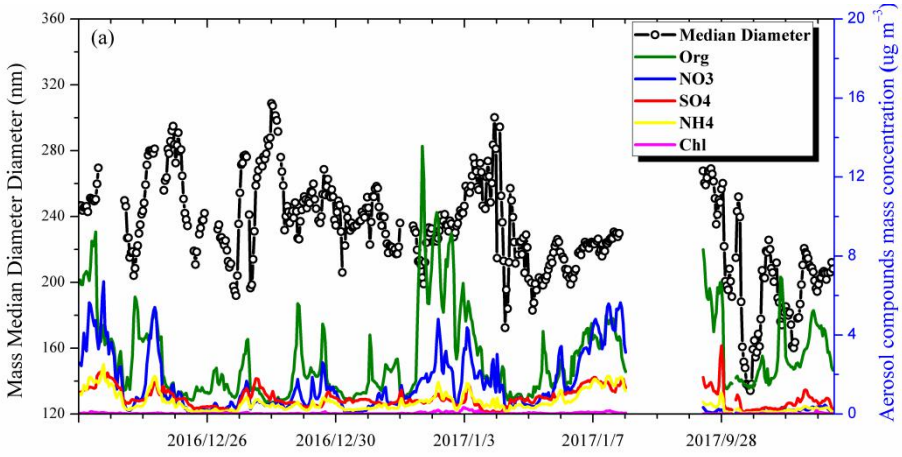

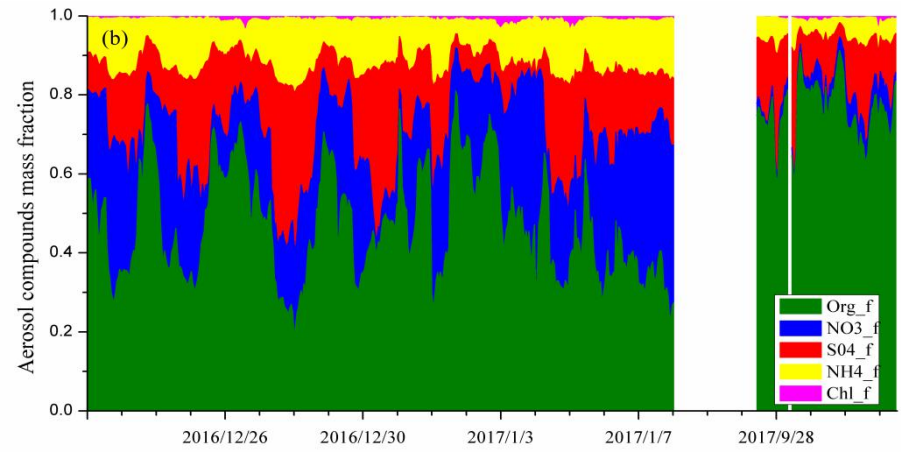

Figure S5. A time series of 1-hour aerosol composition concentration and SMPS mass median diameter (above) with the mass fraction of different chemical species in the composition (below) from 12/22/2016 to 01/07/2017 and from 09/27/2017 to 10/01/2017.

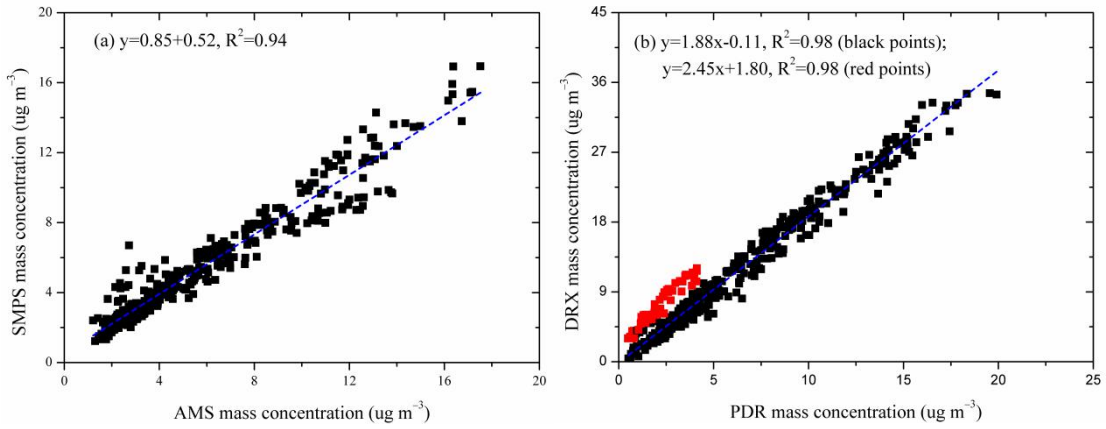

Figure S6. (a): A scatterplot showing correlation of SMPS measurements to concurrent AMS measurements, and (b) : correlation of DRX measurements to concurrent PDR measurements.

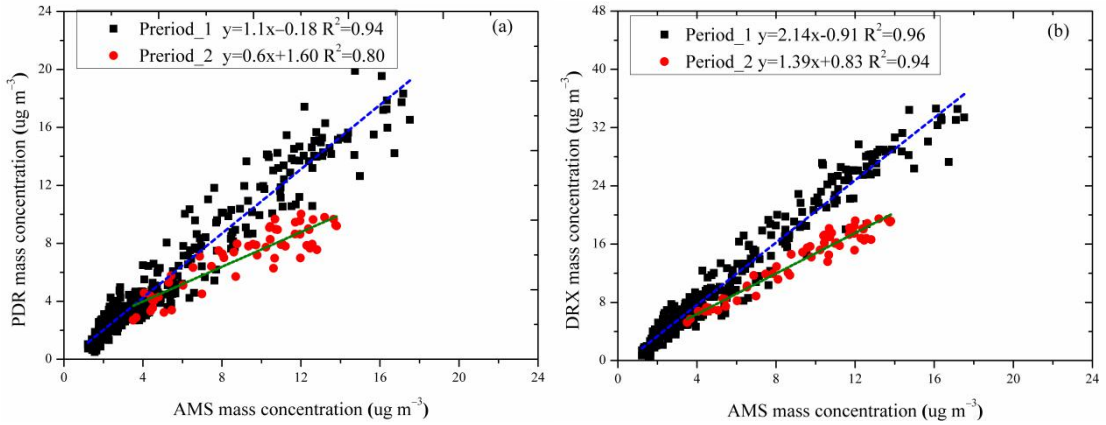

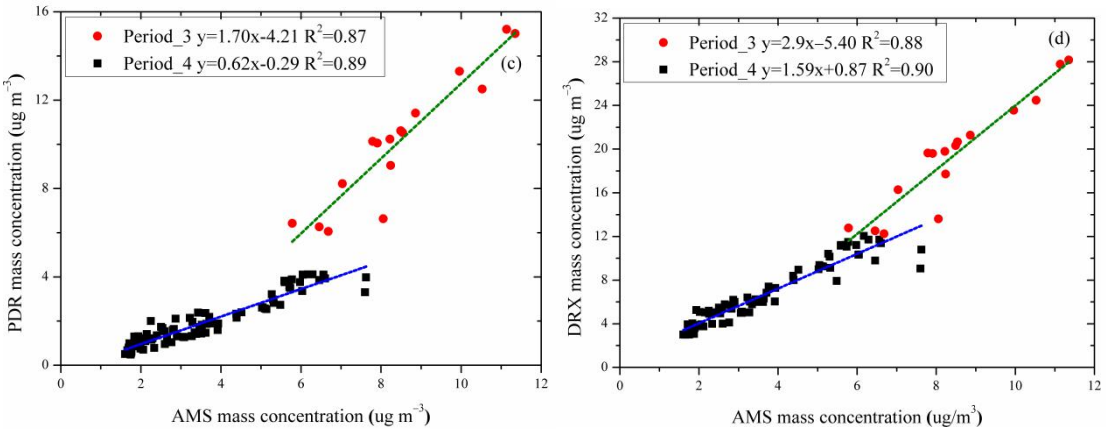

Figure S7. Scatter plots showing correlation between optical instruments measurements to AMS measurements for four sample analysis periods.

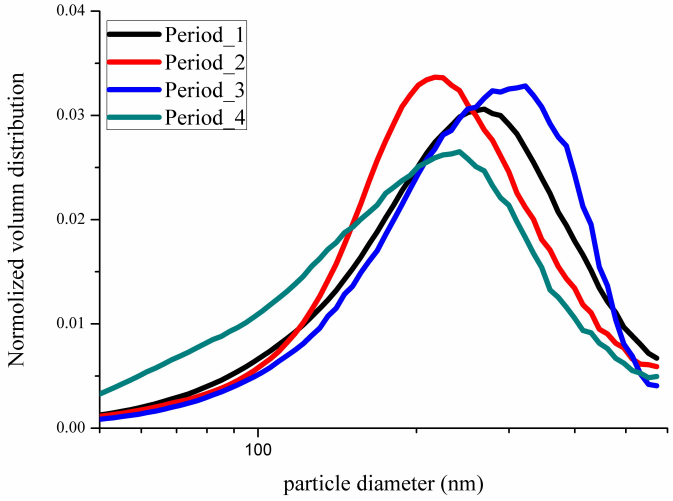

Figure S8. Averaged normalized volume size distribution of ambient aerosol of four periods measured by SMPS.

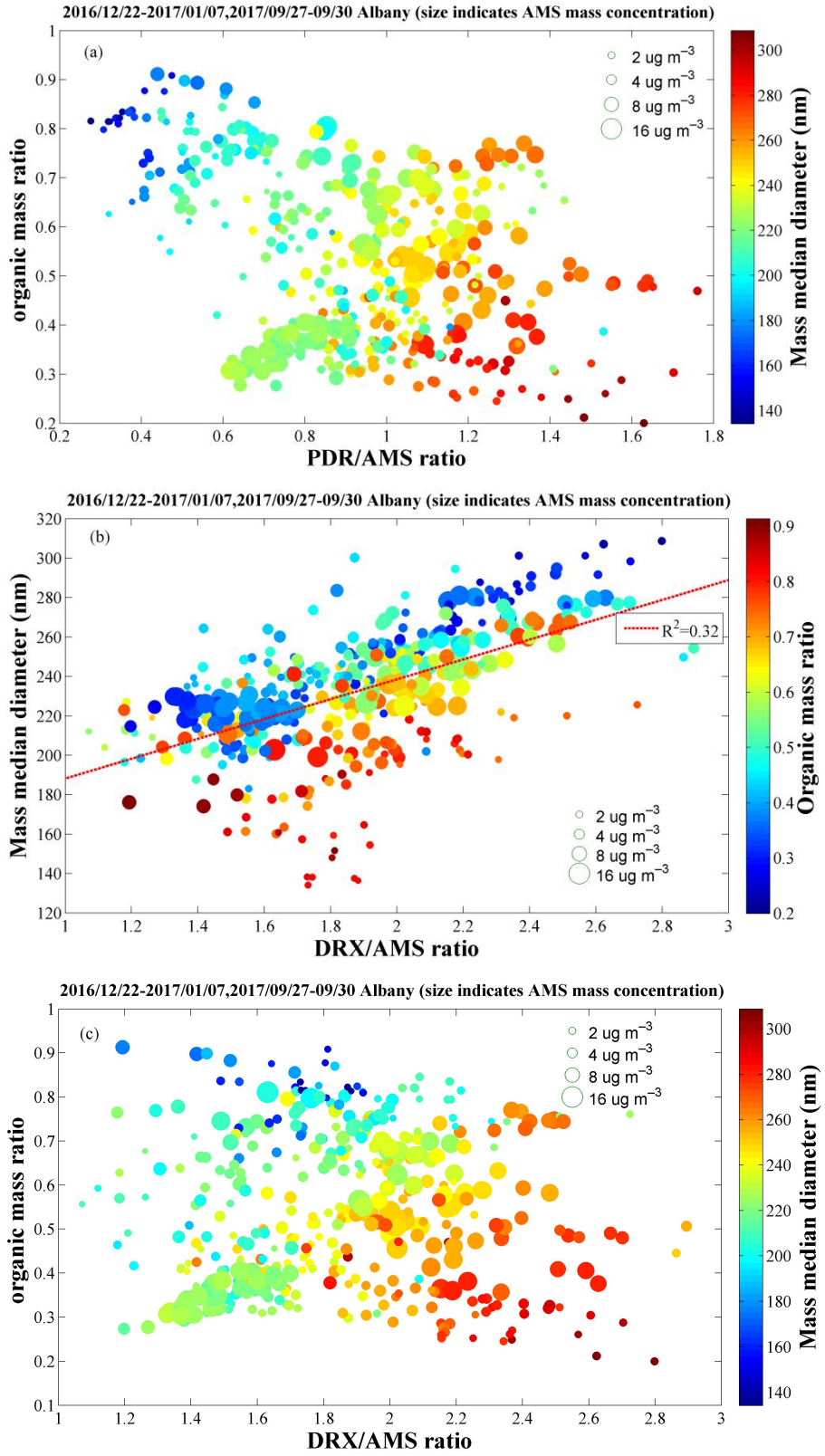

Figure S9. (a): Scatterplot of organic mass fraction and the PDR/AMS ratio. And points are color-coded by aerosol median diameter. (b): Scatterplot and correlation of aerosol median diameter with the DRX/AMS ratio. And points are color-coded by organic mass fraction. (c):

Scatterplot of organic mass fraction with the DRX/AMS ratio. And points are color-coded by aerosol median diameter. All points are sized by AMS mass concentration.

In Fig. S9 the correlation between aerosol median diameter with the DRX/AMS ratio was lower than with PDR/AMS, with the most deviated points the result of primarily small diameter particles located in period_4. One possible reason for the low correlation coefficient with DRX is that particles in period_4 were with smaller size than other periods, and the aerosol with diameters smaller than 100 nm would cause significant bias to DRX, due to its size detection limit. After excluding the points of period_4, the r^2 increases to 0.52, which demonstrates the positive effect of aerosol size on optical instrument response.

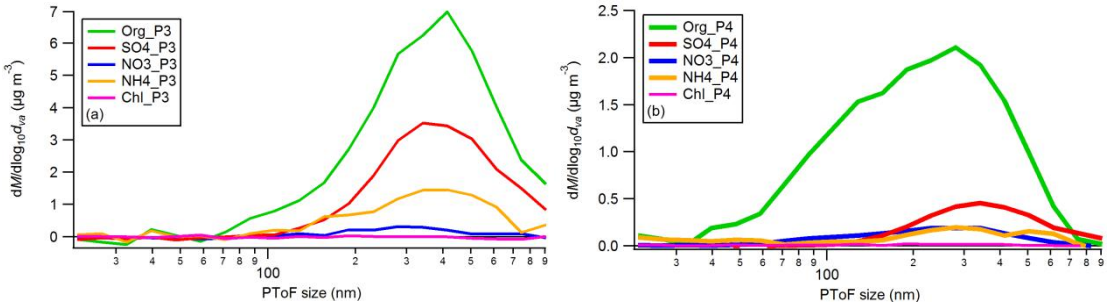

Figure S10. (a): Averaged mass size distribution of aerosol composition during period_3, and (b): averaged mass size distribution of aerosol composition during period_4.

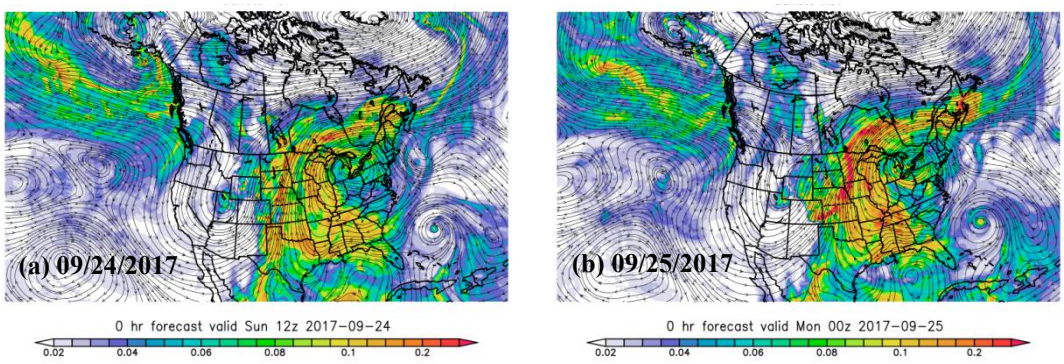

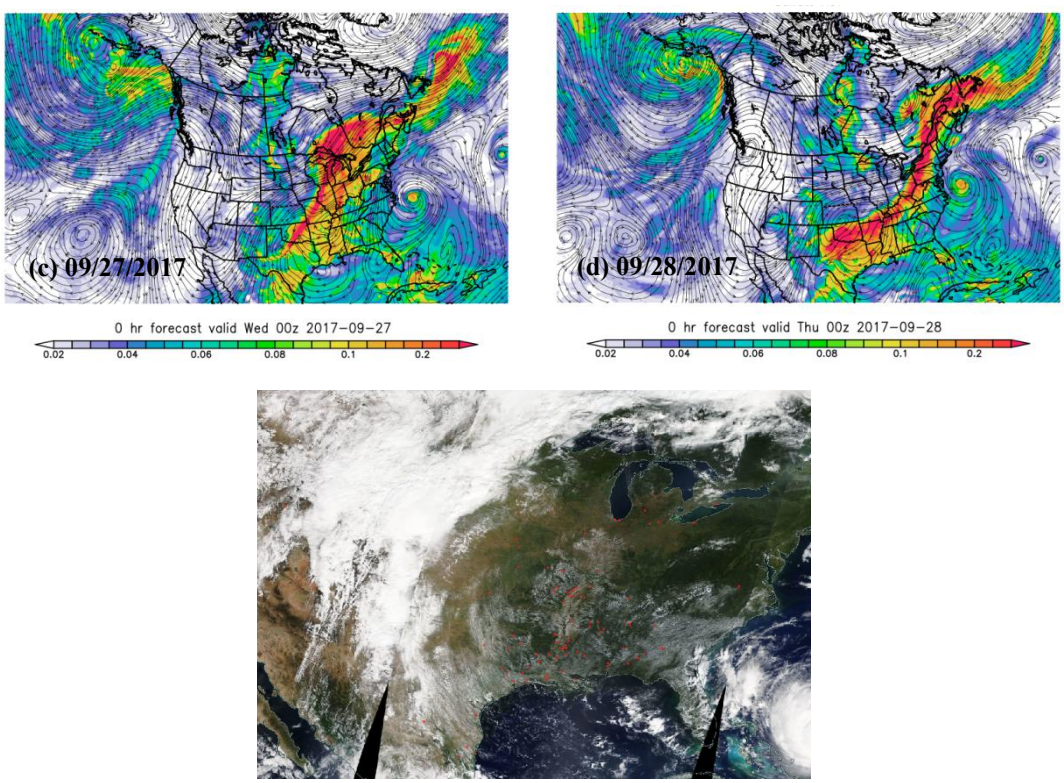

(e) the map of fires and thermal anomalies from Terra and MODIS

Fig. S11. GEOS-5 forecasts for the spatial distribution of sulfate aerosol AOT over North America (https://portal.nccs.nasa.gov) on 09/24/2017, 09/25/2017, 09/27/2017, and 09/28/2017 (above four), and the map of fires and thermal anomalies from Terra and MODIS (https://worldview.earthdata.nasa.gov) on 09/23/2017

It is believed that the sulfate aerosol originated from the lower Mississippi Valley on 09/24/2017, as a result of multiple point-source fires clustered in the region. As time progresses, the sulfate aerosol distribution changed with synoptic downstream flow, and created the prominent band that passes over New York State on 09/28/2017. During this process, the aerosol was believed to have experienced long-period time-sensitive and transport-sensitive chemical reactions.

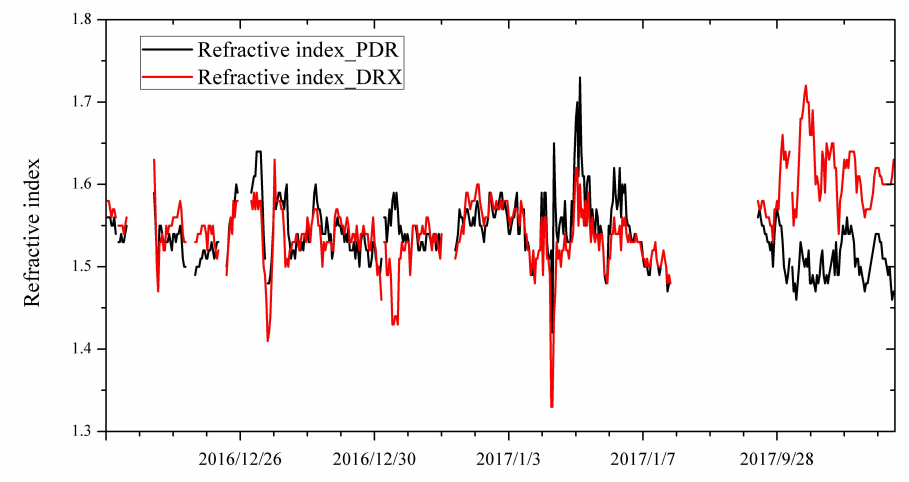

Fig. S12. Time series of estimated aerosol refractive index from PDR and DRX.

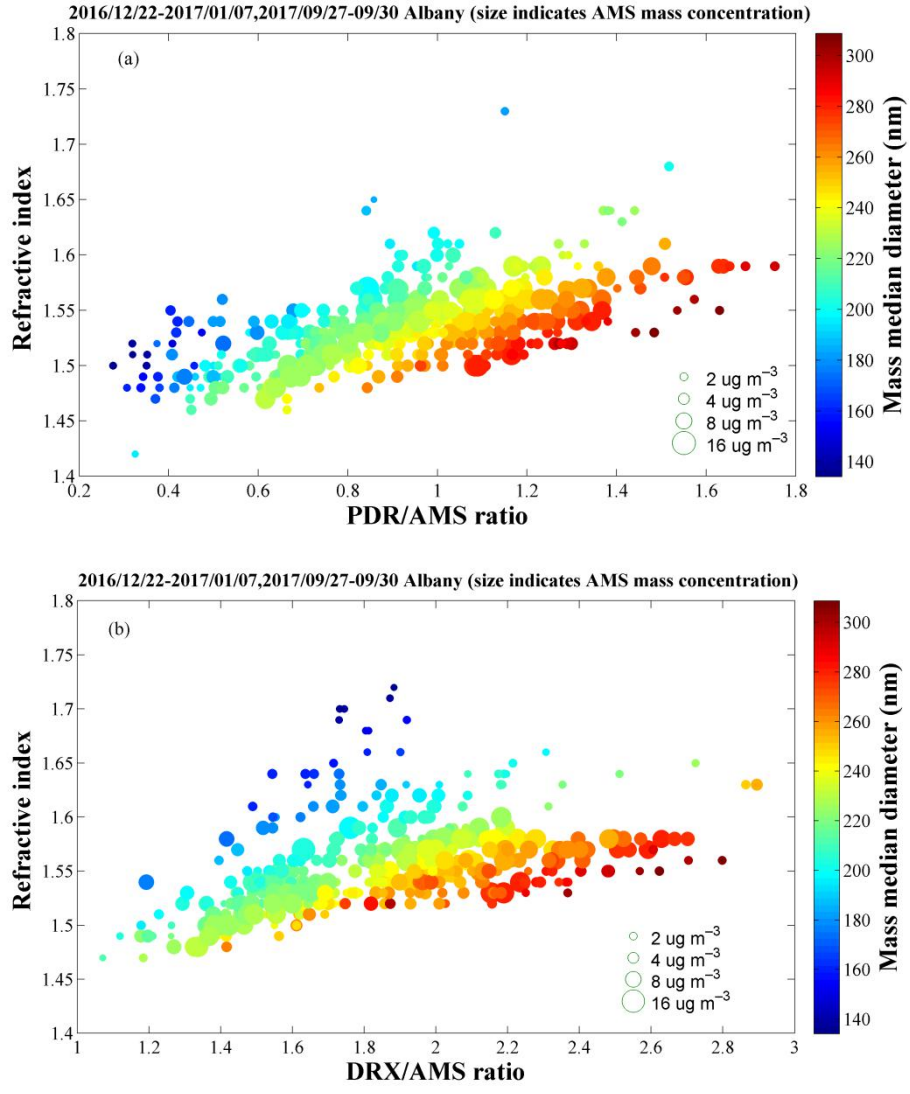

Figure S13. (a): The correlation scatters of aerosol refractive index and the PDR/AMS ratio. (b): The correlation scatters of aerosol refractive index and the DRX/AMS ratio. All points are color-coded by aerosol median diameter, and sized by AMS mass concentration

S3 Tables

Table S1. List of different dilution concentrations for each compound in the three test groups.

Compound	Group 1	Group 2	Group 3
$NaNO_3$ (g L^{-1})	0.75	3	6
$(NH_4)_2SO_4$ (g L^{-1})	0.75	2.5	5
Sucrose (g L^{-1})	0.45	1.5	3
Adipic Acid (g L^{-1})	0.4	1.0	2.5
Median Diameter (nm)	153	202	231

Table S2. Calculated relative Mie scattering flux of the four particle species ($(NH_4)_2SO_4$, $NaNO_3$, sucrose, adipic acid) analyzed by the PDR and DRX, and different dilution concentrations (#1 indicates Group 1; #2 indicates Group 2; #3 indicates Group 3).

Relative flux	$(NH_4)_2SO_4$	$NaNO_3$	sucrose	adipic acid
DRX(#1)	3.37	2.56	3.34	2.50
DRX(#2)	4.72	5.04	5.04	3.19
DRX(#3)	5.41	5.54	5.54	3.72
PDR(#1)	0.79	0.59	0.86	0.69
PDR(#2)	1.31	0.93	1.45	0.96
PDR(#3)	1.59	1.03	1.67	1.24

Table S3. Reference table RF for different refractive indices (TP refers to the time point for each hour of data, wavelength=880 nm, angle=90°)

Index/RF	TP1	TP2	TP3	TP4	TP5	TP6	TP7	TP...
1.2	0.40	0.39	0.39	0.40	0.40	0.41	0.41	...

1.21	0.45	0.43	0.43	0.44	0.44	0.45	0.45	...
1.22	0.49	0.47	0.47	0.48	0.49	0.49	0.50	...
1.23	0.53	0.52	0.51	0.52	0.53	0.54	0.54	...
1.24	0.58	0.56	0.56	0.57	0.58	0.59	0.59	...
1.25	0.63	0.61	0.61	0.62	0.63	0.64	0.64	...
...	...	...	...	...	...	...	...	...
1.75	6.04	5.85	5.73	5.91	6.01	6.06	6.11	...
1.76	6.22	6.02	5.91	6.09	6.19	6.25	6.30	...
1.77	6.41	6.21	6.08	6.28	6.37	6.43	6.49	...
1.78	6.60	6.39	6.26	6.46	6.56	6.62	6.69	...
1.79	6.79	6.58	6.45	6.65	6.75	6.82	6.88	...
1.8	6.99	6.77	6.63	6.84	6.95	7.02	7.08	...

References:

Zhang, Q., Canagaratna, M. R., Jayne, J. T., Worsnop, D. R., and Jimenez, J. L. Time-and size-resolved chemical composition of submicron particles in Pittsburgh: Implications for aerosol sources and processes. Journal of Geophysical Research: Atmospheres, 2005, 110(D7), 2005.

Lee, B. P., Li, Y. J., Flagan, R. C., Lo C., and Chan C. K.. Sizing characterization of the fast-mobility particle sizer (FMPS) against SMPS and HR-ToF-AMS. Aerosol science and technology, 47(9): 1030-1037, 2013.